JOURNAL OF AIRCRAFT
Vol. 34, No. 3, May–June 1997

Rear Fuselage Transonic Flow Characteristics for a Complete Wing–Body Configuration

E. Coustols,* A. Séraudie,* and A. Mignosi†
ONERA, 31 055 Toulouse, France

The study presents results for experiments conducted in the transonic pressurized T2 wind tunnel of Centre d'Etudes et de Recherches de Toulouse. The 1/80th scale model of a modern subsonic transport aircraft was mounted in the test section using a fin-sting. It consisted of a fuselage, a detachable horizontal rear stabilizer, a belly fairing, and tip-truncated wings. The tip-truncated wings were designed by Aerospatiale to reproduce the correct downwash in the rear fuselage region. Tests were conducted at a freestream Mach number of 0.82 and a Reynolds number evaluated with the model chord length of approximately 2.5 × 10^6. Various measurements were performed, mainly in the vicinity of the fuselage downstream rear part: oil-flow visualizations, pressure distributions, boundary-layer surveys along the fuselage symmetry lines and some lateral lines using a laser Doppler anemometry system, and near-wake surveys with both pressure and velocity measurements. These experiments were designed to allow a fine description of the flows developing along the rear part of a fuselage in a configuration similar to actual flight applications.

Nomenclature

$b/2$	=	half wingspan of the model
Cd	=	drag coefficient
Cl	=	lift coefficient
Cl_l	=	local lift coefficient
Cp	=	pressure coefficient $2(p - p_\infty)/(\rho U_\infty^2)$
c	=	local chord length
c_{mac}	=	mean aerodynamic chord length
K_{pr}	=	corrector coefficient for static probe calibration
l	=	fuselage length
M_∞	=	freestream Mach number
p	=	surface pressure
p_{ref}	=	reference static pressure, used only for probe calibration
p_t	=	stagnation or total pressure
$p_{t\infty}$	=	reference stagnation pressure
p_∞	=	reference static pressure
Re	=	Reynolds number, $U_\infty \cdot c_{mac}/\nu_\infty$
RHF	=	reference horizontal fuselage line
S_{ref}	=	reference surface for drag estimation, total wing area at model scale
U, V, W	=	velocity components in the (X, Y, Z) coordinate system
U_∞	=	freestream velocity
X, Y, Z	=	Cartesian coordinates, defined precisely for wake and boundary-layer surveys
α	=	angle of attack
α_{hs}	=	setting of the horizontal stabilizer with respect to RHF
θ	=	azimuthal angle
ν	=	kinematic viscosity
ρ	=	fluid density

Subscripts

e	=	condition at the boundary-layer edge
n	=	direction normal to the wall
pr	=	condition at the probe location
∞	=	condition in freestream flow

Received July 29, 1996; presented as Paper 96-1.3.1 at the 20th Congress of the International Council of the Aeronautical Sciences, Sorrento, Napoli, Italy, Sept. 8–13, 1996; revision received Jan. 15, 1997; accepted for publication Jan. 17, 1997.

*Research Engineer, CERT, Aerothermodynamics Department.
†Head of the Transonic Research Group, CERT, Aerothermodynamics Department.

I. Introduction

EXPERIMENTAL as well as numerical work on rear parts of fuselages have been developed at ONERA/CERT since 1991. The work has several goals:

1) To reach a better understanding of the external and wall flows developing along the fuselage of a commercial-type subsonic aircraft for different model configurations (fuselage without stabilizer, fuselage with stabilizer, and complete wing-body).

2) To generate an important database (pressure distributions, boundary-layer and near-wake surveys with either velocity or pressure measurements or both) necessary for validating inviscid and viscous codes used and developed at ONERA.

3) To forecast possible three-dimensional separation that leads to important viscous drag increase, and, if necessary, to define passive devices as a means to control the flow in the rear-fuselage area.

Subsequent to detailed experimental work on both fuselage without and with horizontal stabilizer,[1,2] a second set of experiments was launched to more closely simulate actual flight applications. A complete wing–body configuration of a modern transonic transport aircraft was considered in these studies. The aim of the experimental approach detailed in this paper was to explore the influence of the horizontal stabilizer and the wing lift on rear-fuselage flows and to investigate the interaction between the wake coming from the tip-truncated wings and the boundary layer developing along the fuselage.

The experiments were conducted in the test section of the CERT T2 wind tunnel, which is transonic, pressurized, and is equipped with self-adaptive walls. Tests were performed at a stagnation pressure close to 2.1 bar, ambient temperature, and a freestream Mach number of 0.82. The Reynolds number, based on the mean aerodynamic chord length of the model, was approximately 2.5 × 10^6. Although the observed Reynolds number was one order of magnitude less than those corresponding to flight or cruise conditions (~5 × 10^7), the value is in perfect agreement with those recorded among the numerous industrial wind-tunnel applications (~4 × 10^6 to 5 × 10^6 for a 1/20th scale model in the ONERA S1 Modane-Avrieux wind tunnel). Furthermore, rear fuselage drag is not significantly affected by either compressibility or Reynolds

number effects, contrary to skin friction component. An empirical method, based on such a hypothesis, has been developed to provide a reliable prediction of the increment in drag coefficient caused by rear fuselage upsweep.[3] It has been, among other studies, validated by Aerospatiale for fuselage alone and wing–body configurations, at given wind-tunnel conditions.

To detail the rear fuselage flow characteristics, multiple measurements were performed: oil-flow visualizations, pressure distributions, boundary-layer surveys along the upper and lower symmetry lines using the three-dimensional laser Doppler anemometry (LDA) system, and wake surveys with both pressure and velocity measurements in two planes located at approximately one and two diameters downstream of the fuselage base.

II. Wind-Tunnel Conditions

A. Experimental Setup — Model

1. T2 Wind Tunnel at CERT/DERAT

The T2 wind tunnel is a closed-circuit, induction-driven facility capable of runs between 30–120 s. It is pressurized, transonic, and cryogenic, and is equipped with self-adaptive walls. Dry air is injected at ambient temperature and cooled by an injection of liquid nitrogen at cryogenic conditions.[4] The standard operating range is Mach number, 0.6–0.9; stagnation pressure, 1.3–3.0 bar; and stagnation temperature, 120–300 K.

The test section of the wind tunnel measures 0.39 m wide, 0.37 m high, and 1.42 m long. The flexible top and bottom walls serve to avoid transonic blockage and minimize wall interference effects. These walls can be controlled using either a two- or three-dimensional strategy[5,6]; the three-dimensional strategy has been considered for all configurations presented in this paper. The walls are moved by 16 hydraulic jacks acting upon invar steel sheets, allowing displacement in 0.2-mm increments up to a maximum variation of 25 mm. The tunnel's adaptive wall capability allows the study of relatively large models and provides very accurate measurement readings.

In addition to reaching high Reynolds number values, the wind tunnel is suitable for studying rear fuselage flow because the three-dimensional LDA system[7,8] provides a means of recording detailed secondary fields that are crucial for identifying vortex flows.

2. Model

The 1/80th-scale model of a modern transonic transport aircraft was designed and manufactured at ONERA/IMF Lille. It consists of a fuselage, a detachable horizontal rear stabilizer, a belly fairing, and tip-truncated wings. The fuselage is 0.733 m long and the diameter of the cylindrical part is 0.070 m. The model differs from the full-scale aircraft in that there is no horizontal stabilizer shield nor gap between the horizontal stabilizer and the fuselage; moreover, the shape of the belly fairing is not exactly the same as the full-scale aircraft and there is no wing/fuselage fillet. Subsequent in-house experiments served to confirm that these small modifications did not affect the main characteristics of the rear-fuselage flow. However, the absence of gap could potentially impede a flow connection between the lower and upper parts of the fuselage.

The actual wing modeled at the selected scale could not be considered because of size constraints in the wind-tunnel cross section. Therefore, tip-truncated wings with exactly the same chord length at the wing/fuselage junction, were designed by Aerospatiale.[9] For correct qualification of the aerodynamic flowfield on the fuselage rear section, the model wings had to be designed so that the pressure field on the fuselage and the position of the wake of the wing on the fuselage duplicated those associated with the real wing at the wind-tunnel conditions. The computed spanwise load distributions are illustrated in Fig. 1 for both real wing under flight conditions and tip-truncated wing under wind-tunnel conditions, referred to as target load and final load, respectively. The correlation is very good between both distributions, which ensures a very consistent downwash on the fuselage, satisfactory coincidence of the wing wake shape on the fuselage and, consequently, a very correct representation of the aerodynamic field on the rear fuselage section, in spite of compromised wing size. It could also be noted it has a rather good consistency with experiments as will be discussed in Sec. III.A.

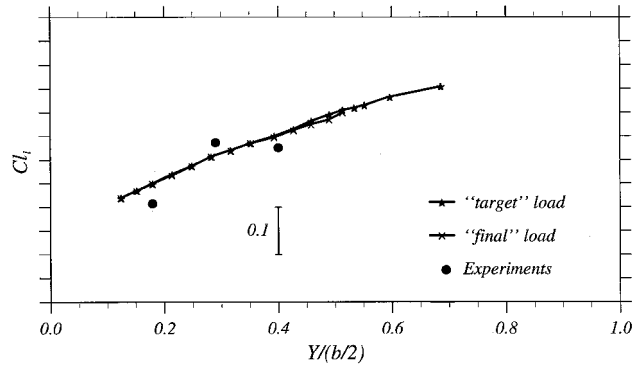

Fig. 1 Spanwise load distributions over both real wing and tip-truncated wing.

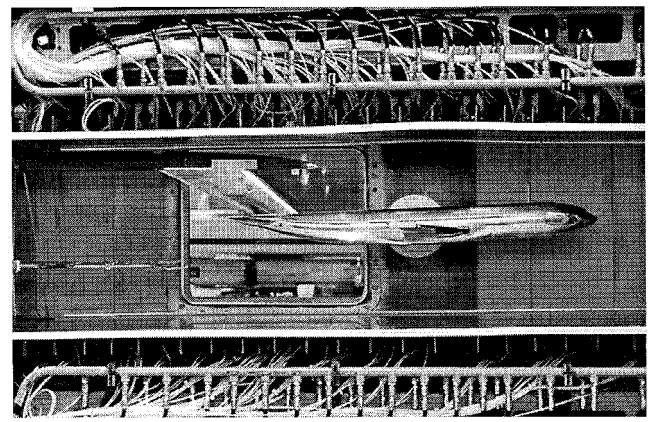

Fig. 2 View of the model in the T2 test section.

3. Experimental Setup

The model was mounted in the test section using the same fin-sting as the one used for the fuselage with or without stabilizer configurations[1,2] (Fig. 2). The model fin was geometrically different from the full-scale aircraft fin, but both the chord at the fuselage/fin junction and the sweep angle of the leading edge were exact.

The sting-induced interferences along the centerline of the wind tunnel in the location of the upswept rear fuselage, but the tunnel's flexible upper and lower walls provided a means of canceling the interference along the fuselage axis. Velocity measurements made during this stage of the experiment verified that the residual disturbances were small.[6] Details regarding wall adaptation are discussed in Sec. II.C.

4. Instrumentation

The model's fuselage (cylindrical part as well as belly fairing) was fitted with 142 static pressure taps, 115 of which were located on the left-hand side of the rear part, along the last 32% of its fuselage length. For two streamwise sections, taps located in the same horizontal plane helped verify that the model was not mounted askew. By recording multiple pressure measurements in this downstream part of the fuselage, it was possible to define, fairly exactly, both the streamwise evolution of pressure along the symmetry lines and the azimuthal distri-

bution of the pressure. These definitions proved critical in the examination of the influence of the horizontal stabilizer on the external flow.

The lower and upper sides of the left tip-truncated wing contained 44 pressure taps, distributed in three sections, located at 65, 105, and 145 mm from the fuselage axis. The corresponding local chords were 117, 96.6, and 84.5 mm, respectively.

A specific pressure rake was constructed for wake surveys. It provided coverage of the entire wake plane survey during a single run. The rake was 84 mm wide, with two decks: the upper one consisting of 15 total pressure probes and the lower one had six static pressure taps. All of the probes were set at equal distance from one another. The total pressure values were measured by a Pressure Systems Incorporated system using individual transducers without any correction; however, some additional corrections were applied to the static values because of the obstruction attributable to the rake.

For every tested Mach number, a calibration of the six static pressure probes was made with an adapted empty test section. A corrector pressure coefficient, independent of M_∞, was defined for each probe: $K_{pr} = (p_{pr}/p_{ref} - 1)/[(\gamma/2)M_{ref}^2]$, where p_{pr} was the measured static value and p_{ref} and M_{ref} were the reference parameters. For the calibration, those latter parameters were deduced from the adaptation procedure ($p_{ref} = p_\infty$, $M_{ref} = M_\infty$). During the model tests, p_{pr} was measured and corrected with the previously cited K_{pr} value to reach the static pressure that would exist at the location of the static probe, without the presence of the rake. The magnitude of such a correction was approximately 2%. Imperfections of the static pressure probes were also taken into account by this correctional technique.

A three-dimensional LDA system was used for boundary-layer and wake surveys. The diameter of the measuring volume (intersection of the three colored beams and their waists) was approximately 130 μm for either forward- or backward-scattering modes of operation. For near-wall measurements, one could approach as close as 0.3–0.4 mm to the wall using the forward-scattering mode (the tangential approach, for the symmetry lines of the model). However, in the backward-scattering mode (normal approach, midlateral line on the fuselage), the shortest distance to the wall was 3.0 mm.

B. Test Conditions

Tests were carried out at a stagnation pressure of 2.1 bar, an ambient temperature of 300 K, and a freestream Mach number of 0.82, resulting in a Reynolds number Re (based upon the mean aerodynamic chord length of the model), of approximately 2.5×10^6.

Transition was controlled by attaching roughness trips on the fuselage (a carborundum band 12 mm from the nose, with an average height of 45 μm), on the lower and upper sides of the horizontal stabilizer (a carborundum band at 5% of the local chord length, with an average height of 35 μm), and on the lower and upper sides of the wings (a carborundum band at 5% of the local chord length, with an average height of 45 μm). Natural transition was allowed to occur on the vertical fin.

For these sets of experiments, the fuselage axis was set at $\alpha = 2.5$ deg and the horizontal stabilizer was set at $\alpha_{hs} = -2$ deg with respect to the RHF. The configuration is representative of the average cruise conditions.

C. Wall Adaptation Process and Measurements

To reproduce the freestream conditions around the model as accurately as possible, a three-dimensional adaptation of the top and bottom walls was performed according to methods developed at DERAT.[5,6] This adaptation was based upon the three-dimensional method developed by Wedemeyer et al.,[10,11] which approximates the flow by a linear potential equation; moreover, the model and its support are assumed to be represented by sinks and vortices located in the neighborhood of

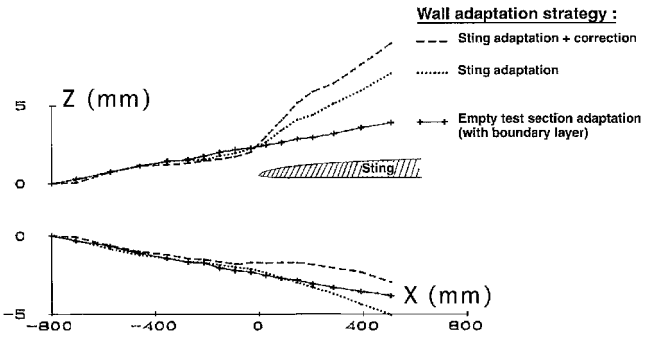

Fig. 3 Correction of sting interference via three-dimensional adaptation.

the centerline of the test section. The side walls are parallel, and the adapted upper and lower wall shapes are calculated to cancel wall interferences along the fuselage axis (near the test section centerline). As input such a method needs the measured upper and lower wall shapes as well as the pressure distributions along the center of both upper and lower walls; therefore, no model representation is needed.

A divergence corresponding to the growth of the four wall boundary layers is added to the calculated shapes. Because of the previously mentioned method, the model and its support are adapted together; nevertheless, the sting produces an interference on the rear part of the fuselage. To minimize that effect the design of the sting was improved and, the adaptation method was modified.

The sting interference has been calculated along the fuselage centerline. The order of magnitude of the maximum downwash deflection is 0.3 deg, with a velocity perturbation of the order of 0.2%. The principle of this modified method is based upon a linearity assumption for the flow and to add to the standard adapted wall shape a correction that cancels the sting interference along the test section axis.

A test was carried out to validate this method: the sting alone was mounted in the test section. The T2 laser velocimetry bench was used to qualify the remaining interference along the test section axis after a standard adaptation procedure. It is therefore worth mentioning that the measured interference was consistent with the computed one. Then, the shape of the walls was determined to create the opposite of the sting interference and was added to the previous standard adapted wall shape, giving the final wall deflections for the experiments (Fig. 3). That leads to a very small flow deviation in the section; thus, uniform flowfield was obtained in the test section in spite of the presence of the sting.

To counteract the wing lift and the induced downwash, the displacement of the flexible walls had to be greater than for the fuselage alone with stabilizer configuration. Great care was taken to ensure the correct pressure distribution on the model as well as the quality of the results.

Following these adjustments, multiple measurements were obtained including oil-flow visualizations on the rear part of the fuselage, on the tip-truncated wings, and on the horizontal and vertical stabilizers; streamwise pressure distributions on the rear part of the fuselage along the upper and lower symmetry lines and on the tip-truncated wings in an azimuthal pattern at selected streamwise sections; boundary-layer surveys at several streamwise abscissas along the symmetry lines of the model using the forward-scattering LDA mode and for several azimuthal positions using the backward-scattering LDA mode; and wake surveys of both velocity and pressure measurements in two planes located at approximately one and two diameters downstream of the fuselage base. For the velocity measurements, a complete plane (~1100–1200 points) was investigated at 60 mm downstream of the fuselage base. A second reading with half of the measurement points (500–600)

was made in one-half of the wake in a plane located 120 mm downstream of the base.

III. Results and Discussions

A. Pressure Field

The streamwise distributions of the pressure coefficient over the tip-truncated wings are plotted in Fig. 4 at three spanwise sections: Y = 65, 105, and 145 mm from the fuselage axis. These distributions are in agreement with those recorded by industrial companies on wing–body models for comparable test conditions, verifying that the adaptation process was applied correctly and that the tip-truncated wings were well designed.

Pressure measurements showed the existence of a shock wave on the upper part of the tip-truncated wings (Fig. 4). Local Mach numbers up to 1.5 were recorded. Oil-flow visualizations were also made to complete the flow description and capture the precise location of the shock wave (Fig. 5). Once the shock wave footprint was estimated, the lift coefficient was computed at the three previously cited sections. Though that coefficient could not be very precisely determined because of few pressure taps, the correct trend was obtained when comparing to the computed lift distributions (cf., Fig. 1).

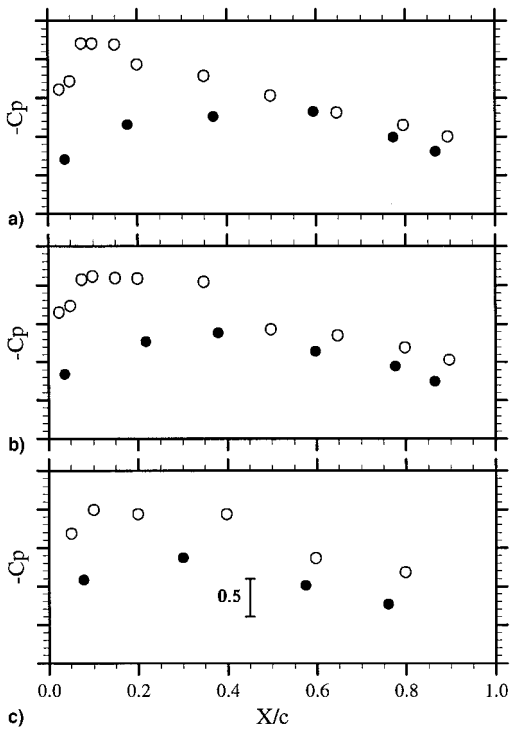

Fig. 4 Pressure distribution on the tip-truncated wing: a) Y = 65 mm [$Y/(b/2)$ = 0.179], b) Y = 105 mm (0.290), and c) Y = 145 mm (0.400). ○, upper side and ●, lower side.

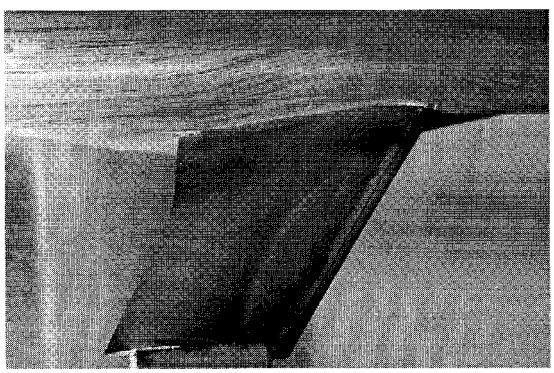

Fig. 5 Oil-flow visualization on the tip-truncated wing.

The concentrations of pressure taps on the rear part of the fuselage created a clear picture of the pressure field in that region. Plots of the contours of constant pressure coefficient are shown in Fig. 6. Comparisons have been made with the configuration without wings and belly fairing, but at two different values of the angle of attack of the model, i.e., α = 2.5 and 0 deg.

Regardless of the configuration, the flow decelerated just ahead of the leading edge of the fin/fuselage junction. Downstream of that area, the flow accelerated as far as the maximum cross section of the horizontal stabilizer footprint. Comparisons with the fuselage with horizontal stabilizer configuration, setting the model at α = 2.5 deg showed some discrepancies, especially along the lower part of the fuselage. The wings apparently induced such a downwash that the angle of attack of the horizontal stabilizer appeared smaller. However, the agreement between the two experimental pressure distributions was very satisfactory when compared to the configuration with the model set at α = 0 deg (Fig. 6a).

The wing lift influence was clearly visible on the pressure distribution over the fuselage (Fig. 7), and the tip-truncated wings induced a very strong acceleration of the flow. The rear part of the belly fairing slowed the flow at the beginning of the fuselage upsweep, thereby reducing the adverse pressure gradient on the upswept lower part of the fuselage.

Comparisons were performed with inviscid flow computations performed at ONERA. Potential flow was calculated by using a panel method developed at Aerospatiale, a source-vortex method with both skin and skeleton panels having either sources of constant strength or vortices with linear chordwise evolution.[12] Computed pressure distributions are illustrated in Fig. 7. The blanks on the full dark lines refer to either the vertical or horizontal stabilizer footprints. Very good agreement was observed for most of the fuselage and its rear part, confirming that the adaptation procedure had been properly applied.

Some discrepancies were observed along the lower symmetry line, both on the pressure level and on the intensity of the pressure gradient. There were several reasons for these discrepancies. First, there was no coupling between inviscid and viscous calculations. Second, there was a relatively thick boundary layer in the area attributable to the upswept fuselage. Moreover, the streamwise pressure gradient along the lower symmetry line is approximately zero downstream of X/l = 0.8, suggesting that the rapid growth of the boundary layer in that area counteracts the decrease of the fuselage cross section. Both the measured and the computed pressure distributions

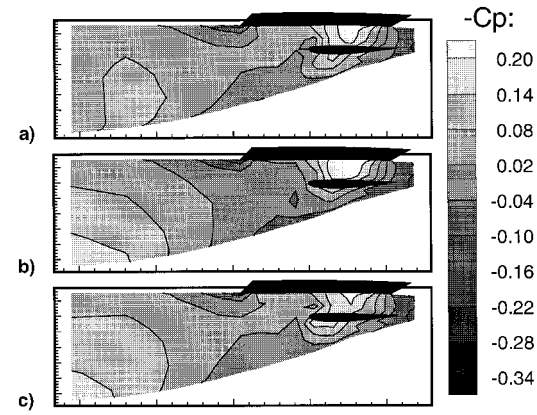

Fig. 6 Contours of constant pressure coefficient on the rear fuselage: a) fuselage alone with horizontal stabilizer configuration: α = 0 deg, α_{hs} = −2 deg; b) fuselage alone with horizontal stabilizer configuration, α = 2.5 deg, α_{hs} = −2 deg; and c) wing–body configuration, α = 2.5 deg, α_{hs} = −2 deg.

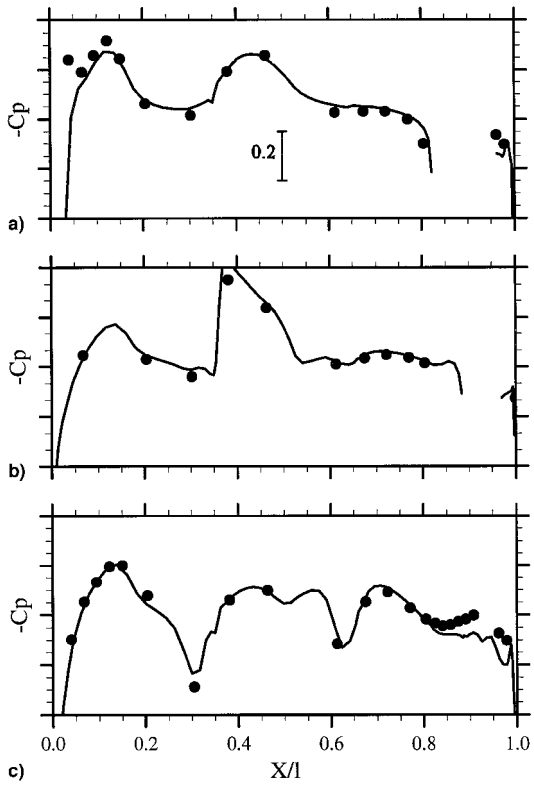

Fig. 7 Pressure distribution along the fuselage: a) upper symmetry line, b) midlateral line (above the wing/fuselage junction), and c) lower symmetry line. ●, experiments—inviscid flow computations.

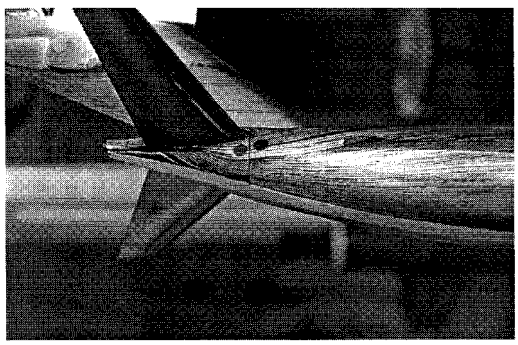

Fig. 8 Oil-flow visualization—view from below.

appear somewhat chaotic around $X/l = 0.93$ (Fig. 7c). This is attributable in part to the local geometrical inflection of the lower symmetry line.

B. Wall Pattern

Oil-flow visualizations were performed on different regions of the model. They provided the evidence necessary to substantiate the efficiency of transition tripping on the tip-truncated wings as well as on the horizontal tailplane, and the splitting of the shock wave on the upper side of the wing (cf., Fig. 5). Furthermore, those visualizations allowed for the precise definition of the wall flow pattern along the fuselage. The following salient features could be observed in Fig. 8: a rather strong deviation of wall streamlines in the cylindrical part of the model, attributed to the wings; a dark triangle area on the lower side of the stabilizer, where oil could gather because of low friction; and a rather strong convergence of wall streamlines inducing an upward motion of wall flow from the lower symmetry line toward the maximum cross section of the horizontal stabilizer. Such a motion gave rise to a vortex roll-up, the source of which is the upsweep. Its vertical development was restricted because of the tailplane.

C. Wake Surveys

Pressure and velocity measurements were recorded in two wake planes orthogonal to the direction of the freestream velocity X; they are located at 60 and 120 mm downstream of the fuselage base, corresponding to approximately one and two diameters, respectively. In these wake surveys, $Y = 0$ refers to as the symmetry plane of the fuselage; the Z axis completes the coordinate system.

Comparisons of these observations to the configurations without wings, as tested in a preceding entry,[1,2] are now possible in the furthest plane, for which only LDA measurements were previously available.

1. Pressure Rake Measurements

Variation of the stagnation pressure in the wake at 120 mm downstream of the fuselage base is illustrated in Fig. 9b. The following comments can be made:

1) The symmetry of measurements in the wake plane was comparable to the one recorded for the fuselage alone configuration with or without horizontal stabilizer.[1,2]

2) The wakes from the vertical and horizontal stabilizers, as well as from both the fuselage/wing interaction and the fuselage, were clearly observed.

3) The shape of the wake was different from the configurations without wings; however, its size (height, width) was comparable to the geometry of the fuselage and to measurements obtained from the fuselage/tailplane configuration at $\alpha = 0$ deg.

4) Pressure loss downstream of the tailplane was roughly constant and equal to 6–8%.

5) Three different velocity defect pockets were recorded in the fuselage wake. The highest pocket was observed from both the fuselage base and the convergence of wall flow along the upper edge of the flat surface, which allows rotation of the horizontal tail. The average pressure loss was around 15%. The two lowest pockets were symmetrical with regard to the wake axis and appeared to be associated with the vortex roll-up spreading along the lower part of the fuselage. A maximum deficit of nearly 20% was recorded.

6) In the lower part of the pictures, the wake of the wing itself induced variations of stagnation pressure of about 2–3%

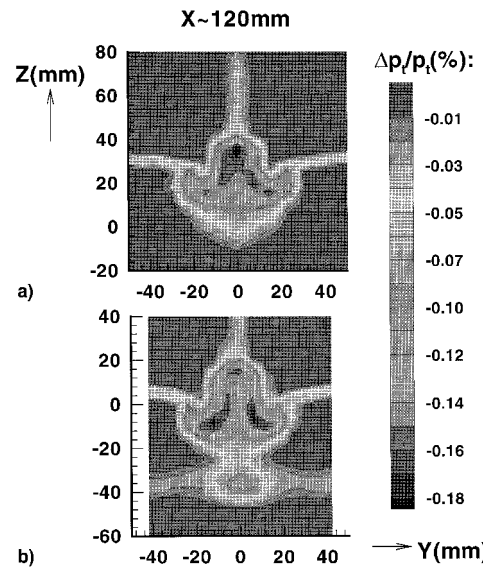

Fig. 9 Contours of constant stagnation pressure loss ($\Delta p_t/p_t$) at two diameters downstream of the fuselage base: a) fuselage alone with horizontal stabilizer configuration, $\alpha = 0$ deg, $\alpha_{is} = -2$ deg and b) wing–body configuration, $\alpha = 2.5$ deg, $\alpha_{is} = -2$ deg.

at approximately 4–5 chord lengths downstream of the wing trailing edge. Nevertheless, a fourth velocity defect pocket of weaker intensity up to 8–10% could be seen under the fuselage: the existence could be attributed to the wake of the vortex that spread from the wing/fuselage junction. Since the wing/fuselage fillet was not present during the tests, the observed pressure loss might not represent the real aircraft situation.

The streamwise evolution of the wake between one and two diameters downstream of the fuselage base did not reveal strong mixing. Of course the intensity of the pressure loss pockets was slightly weaker at the furthest plane, but the location of the pockets within the wake did not change.

When comparing to the case without wings (Fig. 9a), the general shape of the fuselage wake was constant, which is in agreement with the aforementioned similarity of the isobar contours between the two aerodynamic configurations. In the isobars plot, the sharp peak in the upper part of the fuselage wake could be observed in both configurations. It is hypothesized that this peak is related to strong downward negative velocities, as discussed later in this paper.

The same defect velocity pockets existed at roughly the same position within the fuselage wake; however, the intensity appeared somewhat weaker for the case without wings. This observation might be attributed to a stronger vortex roll-up along the lower part of the fuselage attributable to the presence of the wings and its lift.

2. *Three-Dimensional LDA Measurements—Vorticity*

The secondary velocity field has been obtained through LDA measurements (forward scattering) surveys in the Z direction made over a 96 mm height. The lateral step of surveying in the Y direction depends upon the location within the wake plane: 2 mm in the heart of the wake and 3 mm everywhere else.

The secondary velocity field is illustrated in Fig. 10 for the plane located at 60 mm downstream of the fuselage base. It is superimposed on the contours of constant stagnation pressure. It should be noted that both the pressure and the velocity measurements were consistent, and that the flow was perfectly symmetrical. The wakes of every part of the model (fin, tailplane, wings, etc.) were clearly noticeable in the velocity survey. The approximate location of the center of each observed vortex in the fuselage wake will be provided in the following paragraphs with respect to the Y and Z coordinates.

Downstream of the tip-truncated wings and outside of the main wake of the fuselage, there was a noticeable downward motion of fluid related to the overall deviation of the external flow. A convergence of the wake from the wings toward the symmetry plane of the wake of the model was clear. As a consequence, important vertical velocities were recorded in areas with intense vortex activity and small Mach numbers (i.e., where pressure loss was maximum).

Measurements showed the existence of three vortices in each half-wake fuselage plane, compared to two vortices in the configurations without wings. Two vortices were corotating, located not far from the wake axis. They corresponded to vortex roll-up and convergence of wall flow identified along the fuselage, using oil-flow visualizations. The highest vortex ($Y \sim -8$ mm, $Z \sim 10$ mm) is hypothesized to be related to the interference between the tailplane and rear fuselage flows, whereas the lowest one ($Y \sim -10$ mm, $Z \sim -2$ mm) is thought to be linked to the rear fuselage upsweep.

A third contrarotating vortex was located above the tailplane/fuselage junction ($Y \sim -22$ mm, $Z \sim 2$ mm). Its interaction with the other two vortices created rather large negative velocity components, justifying the sharp shape on the contours of constant stagnation pressure. Conversely, the junction of the corotating vortices induced a pronounced upward fluid motion along the wake axis.

At the furthest downstream wake plane, the corotating vortices collapsed and produced a unique and markedly stronger

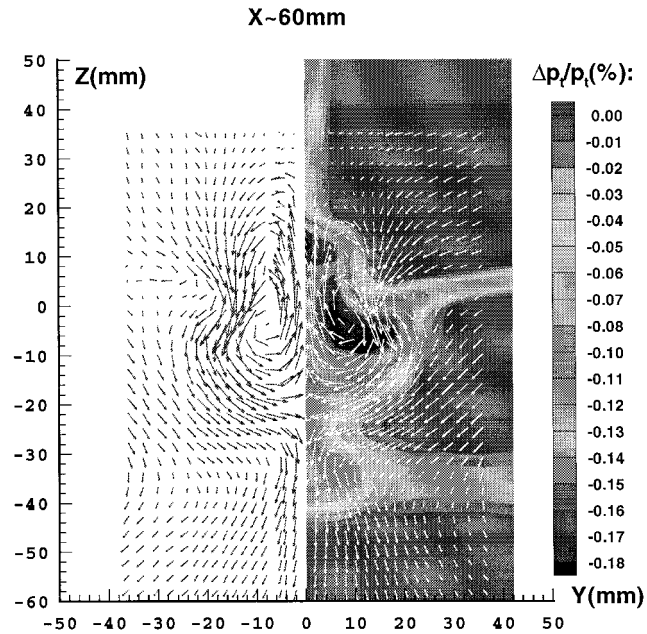

Fig. 10 Secondary velocity field and comparison to the contours of constant stagnation pressure loss ($\Delta p_t/p_t$) at one diameter downstream of the fuselage base.

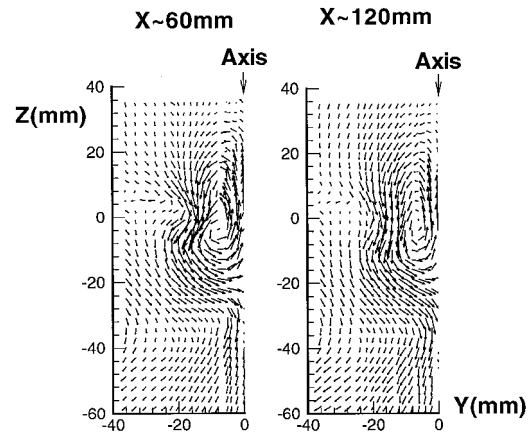

Fig. 11 Secondary velocity field at two streamwise locations downstream of the fuselage base.

vortex (Fig. 11). The secondary velocity plot was then very similar to that recorded in the configuration without wings ($\alpha = 0$ deg $\alpha_{hs} = -2$ deg), although the overall vorticity appears relatively stronger in configurations with tip-truncated wings.

3. *Estimation of Drag Coefficient*

The total drag coefficient of the model was estimated using wake survey data from both velocity and pressure measurements. Indeed, by considering two planes, one upstream of the model (stagnation conditions) and the other one downstream (at 120 mm from the fuselage base), the total Cd was expressed from momentum considerations as

$$Cd = \frac{1}{(1/2)S_{\text{ref}}} \int_{\text{wake}} \frac{\rho U}{\rho_\infty U_\infty} \left(1 - \frac{U}{U_\infty}\right) \mathrm{d}S + \frac{1}{(1/2)\gamma M_\infty^2 S_{\text{ref}}} \int_{\text{wake}} \left(1 - \frac{P}{P_\infty}\right) \mathrm{d}S$$

Table 1 Drag coefficient of the fuselage part only

α, deg	α_{hs} deg	Wings	$10^4 \Delta Cd$	Cd_{vortex}/Cd
0	−2	No	−0.9	1.1%
2.5	−2	No	−5.0	0.2%
2.5	−2	Yes	——	2.6%

where the reference surface is the total wing area at the model scale. By considering only first-order terms, the vortex drag component was

$$Cd_{\text{vortex}} = \frac{1}{(1/2)S_{\text{ref}}} \int_{\text{wake}} \frac{1}{2} \frac{\rho}{\rho_\infty} \frac{(V^2 + W^2)}{U_\infty^2} \, dS$$

To estimate the drag coefficient of the fuselage alone, it was necessary to eliminate the effects of the stabilizers, wings, and belly fairing. Some difficulties occurred, however, because of the strong interaction of these lifting surfaces with the fuselage. Contributions of the fin as well as the tailplane were omitted, using the same method as the one previously developed for the configurations without wings.[1,2] It was very difficult to omit the contribution of the wing/fuselage junction and belly fairing because of the relatively strong interaction with the fuselage. As a result, ΔCd must be expressed as the relative drag variation of the fuselage drag of a given configuration minus the total drag of the complete wing–body configuration (Table 1).

For the configurations without wings, the total drag of the fuselage, primarily pressure drag, was smaller at $\alpha = 2.5$ deg than at $\alpha = 0$ deg because of a decreased relative upsweep angle of the rear part of the fuselage; consequently, the vorticity contribution was also reduced.

The drag coefficient of the fuselage itself, when taking into account the belly fairing and the truncated wings, was similar to the one recorded for the fuselage with horizontal stabilizer configuration, when setting the fuselage at 0 deg. However, the vorticity was stronger than observations recorded without wings, producing almost 3% of the total drag coefficient of the fuselage.

D. Boundary-Layer Surveys

Boundary-layer surveys were performed at different streamwise locations on both the upper and lower symmetry lines or lateral lines, with the LDA system operating in the forward- or backward-scattering mode, respectively.

Profiles were plotted in a coordinate system associated with the boundary layer: y_n is the direction normal to the wall, X and Z are in the plane tangent to the wall, with $Z = 0$ corresponding to the symmetry plane. Mean and fluctuating velocity profiles are discussed at the streamwise locations marked with the solid circles in Fig. 12.

1. *Along the Symmetry Lines*

The LDA system was operated in the forward-scattering mode to obtain better accuracy, better measurement quickness, and a better near-wall approach for these measurements.

On the lower symmetry line, seven measurement stations were defined between $X/l = 0.771$ and 0.980. At each station, probings were made in the direction normal to the wall. Mean velocity profiles are plotted in Fig. 13. The W velocity component in the Z direction did not exceed 5 ms^{-1}, whereas the external freestream velocity was approximately 260 ms^{-1}. Thus, two observations could be verified: 1) the symmetry of the flow is perfect and 2) the measurement volume was correctly positioned.

The wake downstream of $X/l = 0.842$ and coming from the trailing edge of the tip-truncated wings apparently interacted with the mean streamwise velocity component. However, the V component did not seem to be significantly altered. The intensity of the V component was rather strong and was directly proportional to the thickening of the boundary layer attributable primarily to the downwash of the external flow. Downward, near the rear end of the fuselage, the wing-wake separated from the lower symmetry line, thus minimizing the interaction. Therefore the thickness of the boundary layer was as important as the greatest length of the fuselage cross section. The use of boundary-layer codes to predict the viscous flow in that region was questioned.

From these probings it was possible to estimate the wake from the wing/fuselage junction and its interference with the boundary layer developing along the lower symmetry line (as sketched in Fig. 12).

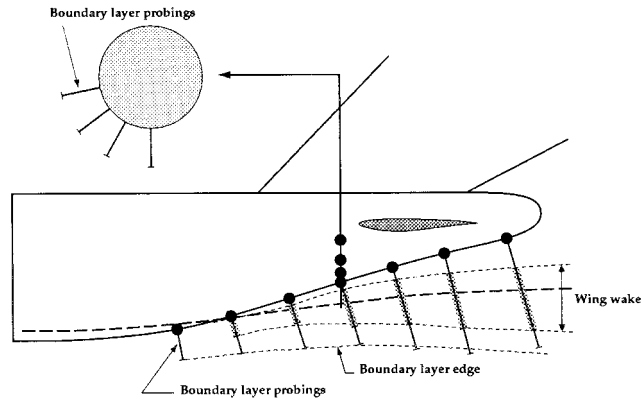

Fig. 12 Locations of some of the boundary-layer surveys.

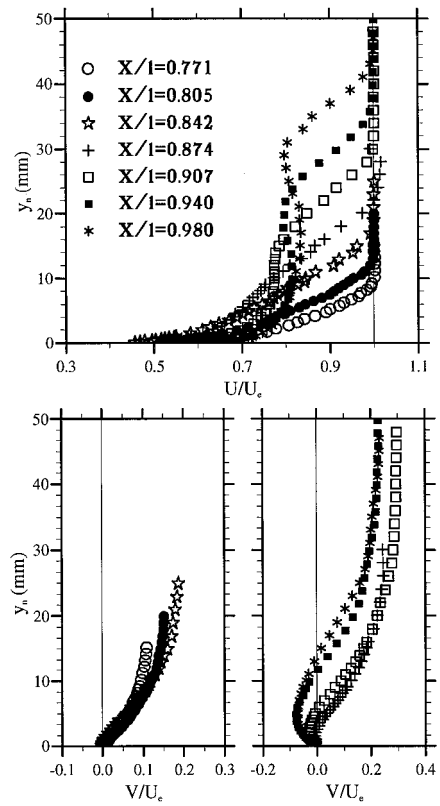

Fig. 13 Streamwise and normal to the wall velocity profiles along the lower symmetry line.

2. *Along Some Lateral Lines*

Boundary-layer surveys were made in different azimuthal lines ahead of and just below the horizontal stabilizer. The location of these stations was judiciously selected according to the wall streamline pattern and in areas of strong convergence of fluid.

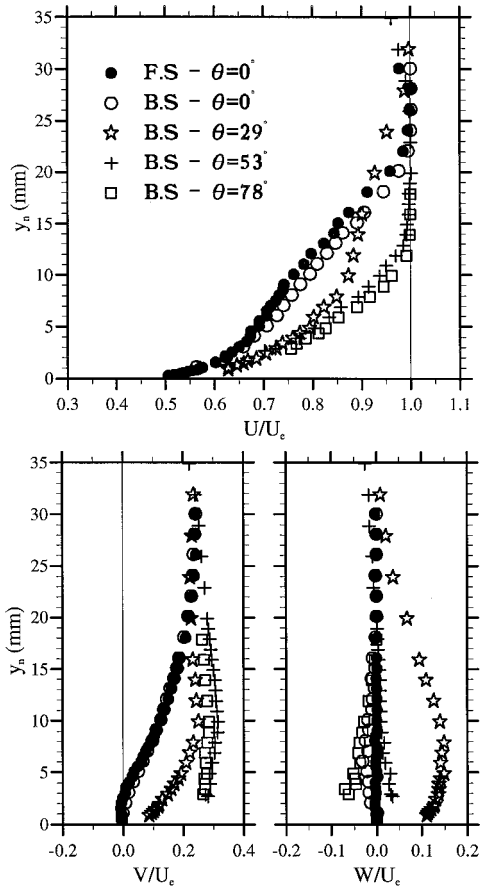

Fig. 14 *X*, y_n, and *Z* components of the mean velocity at *X/l* = 0.874 and different azimuthal locations. F.S, forward scattering and B.S, backward scattering.

The three components of the velocity, computed in the coordinate system associated with the external streamline, are illustrated for various azimuthal angles at *X/l* = 0.874 (Fig. 14). The notations θ = 0 and 90 deg refer to the lower symmetry line and the midlateral line, respectively.

Comparisons were performed between forward and backward scattering on the lower symmetry line, allowing for measurements as close as 1 mm to the wall through backward scattering. The agreement is rather good between these two laser configurations for θ = 0 deg. Some discrepancies existed for the streamwise velocity component. The transverse component *W* was weak but not equal to zero, as symmetry would require. This demonstrates the difficulty in measuring small quantities or transverse velocities through backward scattering. Nevertheless, such a method is of prime importance when dealing with change of sign of crossflow, which was the case between azimuthal angles of 53–78 deg. These surveys provide evidence of both the interaction with the wing-wake and the boundary layer and the rapid thickening of the turbulent boundary layer when moving toward the lower symmetry line. For the high values of θ, in areas where visualizations revealed a strong convergence of wall flow, the *V* component was rather strong.

IV. Conclusions

The purpose of the experiments described herein was to examine the viscous and inviscid flows in the rear part of the fuselage and in the near wake of a wing–body configuration. Detailed information was provided as evidence of the strong interaction between the wake coming from the tip-truncated wings and the boundary layer developing along the fuselage. The effect of the horizontal stabilizer on the wall flow was also characterized using experimental data.

Tests were done in the transonic pressurized wind tunnel with self-adaptive walls of ONERA/CERT, using a 1/80th scale model of a modern transonic transport aircraft. The model consisted of a fuselage, a detachable horizontal rear stabilizer, a belly fairing, and tip-truncated wings. The actual wing sized at the right scale could not be considered because of the size of the wind tunnel cross section, therefore tip-truncated wings were computed by Aerospatiale to reproduce the correct downwash in the fuselage region.

The complete model was mounted in the test section by means of a fin-sting, and was set at an angle of attack of 2.5 deg. The horizontal stabilizer was fixed at −2 deg with respect to the reference horizontal fuselage line. The test conditions consisted of a stagnation pressure approximately 2.1 bar, ambient temperature, and a freestream Mach number of 0.82.

Great care was taken to ensure the correct pressure distribution on the model. The upper and lower flexible walls were moved not only to take into account the presence of the model and of the walls' boundary layers, but also to counteract the disturbance caused by the sting.

The combination of techniques such as oil-flow visualization, boundary-layer surveys, and wake flow measurements provided a means of precise descriptions of the wall flow and of the vortex motion that develops near the lower symmetry line of the fuselage and, subsequently spreads downstream of the upswept fuselage. A tremendous amount of data have been computed for different configurations to support validation or improvement of boundary-layer and Navier–Stokes codes.

Areas of strong crossflow associated with convergence of wall streamlines were identified from oil-flow visualizations. Boundary-layer surveys on specific lines demonstrated the thickening of the boundary layer along the lower symmetry line of the model, as well as an important wing-wake/fuselage-boundary-layer interaction. Rear fuselage flow is generally dominated by three-dimensional separation, i.e., convergence of wall streamlines, the rear fuselage upsweep, creating a lift-induced vortex system amplified by the wing downwash.

In the wake of the model, strong pressure losses were recorded. The use of a three-dimensional LDA system provided a more precise definition of both the vortex system associated with these velocity defect pockets and the intensity of the secondary velocity components in some confined areas of the entire wake. The wake surveys underscore the important and complementary need for pressure and velocity measurements when investigating vortex flows.

In addition to friction or lift-induced drag reductions, benefits can be obtained for transport aircraft applications via reduced fuselage afterbody drag.[13] Future investigations might control the vortex flow by using small passive devices such as vortex generators or small fences. The goal of such experiments would be to act directly on the viscous flow developing between the lateral midline and the lower symmetry line of the fuselage, thereby influencing the flow along the horizontal tail. However, if the desire is to reduce the vorticity drag, whatever its contribution to the drag budget, successful passive devices could potentially modify the pressure and friction drags, thereby producing a greater effect in terms of variations of the total drag of the fuselage. Conversely, benefits for aircraft applications could also be obtained from vortex flow control by reducing and/or confining instabilities that vortices produce.

The tests reported in this paper have been augmented by further experiments using two different kinds of devices: small rectangular fences and small triangular vortex generators. The former drive the external flow and attempt to reset it upward. The latter act upon the wall flow and increase the turbulent mixing between the outer and inner regions of the boundary layer.

The preliminary experiments demonstrate several noteworthy points. First, it is possible to interact with the convergence of wall streamlines and thus flow separation. Second, it is pos-

sible to locally modify the pressure distribution. Finally, it is possible to alter to varying degrees the shape of the wake as well as the distribution of the velocity defect pockets. Whatever configuration is concerned, suppression of the global rear-fuselage vortex system does not seem achievable because the system itself is constrained by the upswept fuselage and cannot be removed without changing the geometrical shape of the rear part of the fuselage. However, our data suggest that it is possible to diminish the potential effects.

Acknowledgments

The authors gratefully acknowledge the support that Airbus Industrie and the Service Technique des Programmes Aéronautiques have provided for the experimental research reported in this paper. They wish to express their gratitude to Jean Cousteix, Head of the Aerothermodynamics Department of CERT, for providing useful comments to enhance the final draft. The first author has benefited greatly from valuable discussions with M. C. Pujol and P. Colin from Aerospatiale, Branche Aéronautique, Toulouse. E. Coustols is also very grateful to the referee who made very pertinent comments that helped improve the earlier version of this paper.

References

[1]Coustols, E., Prudhomme, S., Destarac, D., and Mignosi, A., "Rear Fuselage Flow Studies on a Modern Transonic Transport Aircraft," *Proceedings of the ICAS 19th Congress/AIAA Aircraft Systems Conference*, AIAA, Washington, DC, 1994, pp. 1258–1271.

[2]Coustols, E., Prudhomme, S., Mignosi, A., and Destarac, D., "Rear Fuselage Flow Studies on a Modern Transonic Transport Aircraft," *Journal of Aircraft*, Vol. 32, No. 6, 1995, pp. 1183–1190.

[3]Engineering Science Data Unit, 80006— Aerodynamic Subseries, Royal Aeronautical Society, April 1980.

[4]Séraudie, A., Archambaud, J.-P., Blanchard, A., Dor, J.-B., and Mignosi, A., "T2 Cryogenic Transonic Wind Tunnel Thermal Design and Control of the Facility Including Models Adapted for Short Run Processing," *Proceedings 3rd ASME-JSME Thermal Engineering Joint Conference on Cryogenic Wind Tunnels* (Reno, NV), 1991, pp. 379–386.

[5]Archambaud, J.-P., and Mignosi, A., "The Cryogenic Adaptive Wall Wind Tunnel T2: Quality of the Adaptation with 2D and 3D Strategy, Residual Corrections, Assessment of Sidewall Effect in 2D Cases," International Conference on Adaptive Wall Wind Tunnel Research and Wall Interference Correction, Xian, PRC, June 1991.

[6]Archambaud, J.-P., and Mignosi, A., "Techniques d'Adaptation Tridimensionnelle à la Soufflerie Transsonique T2 de l'ONERA/CERT, DERAT Aerothermodynamics Dept., TR 49/5606.34, April 1992.

[7]Prudhomme, S., Séraudie, A., and Mignosi, A., "A Recent 3D Laser Doppler Application at the T2 Transonic Wind Tunnel: Optimisation, Experimental Results and Measurement Accuracy," 4th International Conference on Laser Anemometry, Cleveland, OH, Aug. 1991.

[8]Mignosi, A., Séraudie, A., and Prudhomme, S., "Applications Tridimensionnelles de la Vélocimétrie Laser en Écoulement Transsonique à la Soufflerie T2," 3ème Congrès Francophone de Vélocimétrie Laser, Toulouse, France, Sept. 1992.

[9]Lépinard, G., and Colin, P., "Design of a Tip-Truncated Wing for a Wind Tunnel Model," Aérospatiale, TR 443.551/91, July 1991.

[10]Wedemeyer, E., and Lamarche, L., "Minimization of Wall Interference for Three-Dimensional Models with Two-Dimensional Wall Adaptation," TN 149, Von Kármán Inst., March 1984.

[11]Wedemeyer, E., and Lamarche, L., "The Use of 2D-Adaptive Wall Test Sections for 3D-Flows," AIAA Paper 88-2041, May 1988.

[12]Rivoire, V., and Eichel, P., "Méthode d'Analyse Tridimensionnelle de Systèmes Hypersustentateurs," Aérospatiale, TR 443.528/87, July 1987.

[13]Coustols, E., "Control of Turbulent Flows for Skin Friction Drag Reduction," *Control of Flow Instabilities and Unsteady Flows*, edited by G. E. A. Meier and G. H. Schnerr, Springer–Verlag, New York, 1996, pp. 155–202.